Title

Seasonal Cycle of Isotope-Based Source Apportionment of Elemental Carbon in Airborne Particulate Matter and Snow at Alert, Canada

Journal

Journal of Geophysical Research: Atmospheres, 125(23)

ISSN

2169-897X

Authors

Rodríguez, BT
Huang, L
Santos, GM
et al.

Publication Date

2020-12-16

DOI

10.1029/2020jd033125

JGR Atmospheres

RESEARCH ARTICLE
10.1029/2020JD033125

Special Section:
The Arctic: An AGU Joint Special Collection

Seasonal Cycle of Isotope-Based Source Apportionment of Elemental Carbon in Airborne Particulate Matter and Snow at Alert, Canada

B. T. Rodríguez[1], L. Huang[2], G. M. Santos[1], W. Zhang[2], V. Vetro[2], X. Xu[1], S. Kim[1], and C. I. Czimczik[1]

[1]Department of Earth System Science, University of California, Irvine, CA, USA, [2]Climate Research Division, Atmospheric Science and Technology Directorate/Science and Technology Branch, Environment and Climate Change Canada, Toronto, ON, Canada

Key Points:
- EC in PM at Alert peaked in winter (135 ng C m^{-3}) and was lowest in summer, a typical seasonal cycle controlled by meteorological conditions
- Biomass burning EC was more important in summer (48–80%) than from fall to spring (30–53%), when liquid and solid fossil sources dominate
- Snow contained more biomass burning EC than PM (53–88% vs. 30–53%); networks undercount biomass burning EC due to complex transport patterns

Supporting Information:
- Supporting Information S1

Correspondence to:
L. Huang and C. I. Czimczik,
czimczik@uci.edu;
lin.huang@canada.ca

Citation:
Rodríguez, B. T., Huang, L., Santos, G. M., Zhang, W., Vetro, V., Xu, X., et al. (2020). Seasonal cycle of isotope-based source apportionment of elemental carbon in airborne particulate matter and snow at Alert, Canada. *Journal of Geophysical Research: Atmospheres*, *125*, e2020JD033125. https://doi.org/10.1029/2020JD033125

Received 26 MAY 2020
Accepted 21 OCT 2020
Accepted article online 18 NOV 2020

Abstract Elemental carbon (EC) is a major light-absorbing component of atmospheric aerosol particles. Here, we report the seasonal variation in EC concentrations and sources in airborne particulate matter (PM) and snow at Alert, Canada, from March 2014 to June 2015. We isolated the EC fraction with the EnCan-Total-900 (ECT9) protocol and quantified its stable carbon isotope composition ($\delta^{13}C$) and radiocarbon content ($\Delta^{14}C$) to apportion EC into contributions from fossil fuel combustion and biomass burning (wildfires and biofuel combustion). Ten-day backward trajectories show EC aerosols reaching Alert by traveling over the Arctic Ocean from the Russian Arctic during winter and from North America (>40°N) during summer. EC concentrations range from 1.8–135.3 ng C m^{-3} air (1.9–41.2% of total carbon [TC], $n = 48$), with lowest values in summer (1.8–44.5 ng C m^{-3} air, $n = 9$). EC in PM ($\Delta^{14}C$ = -532 ± 114‰ [ave. ± SD, $n = 20$]) and snow (−257 ± 131‰, $n = 7$) was depleted in ^{14}C relative to current ambient CO_2 year-round. EC in PM mainly originated from liquid and solid fossil fuels from fall to spring (47–70% fossil), but had greater contributions from biomass burning in summer (48–80% modern carbon). EC in snow was mostly from biomass burning (53–88%). Our data show that biomass burning EC is preferentially incorporated into snow because of scavenging processes within the Arctic atmosphere or long-range transport in storm systems. This work provides a comprehensive view of EC particles captured in the High Arctic through wet and dry deposition and demonstrates that surface stations monitoring EC in PM might underestimate biomass burning and transport.

Plain Language Summary Elemental carbon (EC) aerosols are produced during combustion processes and impact Arctic climate because they absorb light, warm the atmosphere, and accelerate snow and ice melt. Here, we measured the concentration and isotopic composition of EC suspended in the atmosphere and in snow at Alert, Canada, between March 2014 and May 2015. We found that concentrations were lowest during the summer and increased throughout the winter and early spring. This pattern is typical, because EC is removed from the atmosphere by precipitation, which happens more frequently during summer. Our isotope data and meteorological analyses revealed that fossil fuel burning in the Russian Arctic was an important source of EC to Alert from September to May, while forest fires in the North American boreal region were major sources of EC during the summer. We also found that snow contained a greater proportion of EC derived from biomass burning than the suspended aerosols. Snow might be preferentially capturing biomass burning EC from the local atmosphere or be transporting them to the Arctic from lower latitudes. Since EC surface observing networks routinely measure EC in PM but not snow, the impact of biomass burning EC sources on Arctic climate might be underestimated.

1. Introduction

Aerosol influences Arctic climate via aerosol-radiation and aerosol-cloud interactions (Willis et al., 2018). A major contributor is carbonaceous aerosol that mostly consists of weakly refractory, light-scattering organic carbon (OC) and a smaller fraction of strongly refractory, light-absorbing elemental carbon (EC), also "black carbon" (Andreae & Gelencsér, 2006; Petzold et al., 2013; Pöschl, 2005). OC can be emitted during combustion processes as primary aerosols and also as secondary aerosols from the oxidation and condensation of volatile organic compounds (Hallquist et al., 2009), whereas most EC is directly emitted during

combustion processes. Suspended within the atmosphere and deposited on snow- and ice-covered surfaces, EC impacts climate directly and indirectly (Bond et al., 2013).

Arctic aerosols arise from the long-range transport of pollutants into the Arctic from lower latitudes and emissions within the Arctic (Willis et al., 2018). Their concentrations, composition, life-time, sources, and climate impacts vary seasonally due to shifts in available solar radiation, temperature, and precipitation (Law & Stohl, 2007). The aerosol burden is greatest in winter and spring, known as "Arctic haze" (Law & Stohl, 2007; Shaw et al., 1993). Its vertical distribution within the atmosphere is bimodal (Hansen & Rosen, 1984), and satellite observations show that regionally emitted pollutants accumulate below strong inversions within the polar dome in winter, while pollutants from lower latitudes reach the free troposphere in spring (Qi & Wang, 2019; Thomas et al., 2019). Surface pollution episodes arise from stagnant conditions caused by high-pressure systems and inefficient scavenging of particles within the polar dome (Browse et al., 2012; Qi, Li, Henze, et al., 2017; Shen et al., 2017).

Concentrations of air pollutants such as EC have been decreasing at various Arctic monitoring stations due to an overall decrease in emissions (Dutkiewicz et al., 2014; Hirdman et al., 2010). However, we anticipate changes in the concentration and composition of Arctic aerosol (Willis et al., 2018) as a consequence of rapid climate change (Box et al., 2019), diminishing sea ice (Comiso, 2012), changes in the productivity and disturbance regimes of marine and terrestrial ecosystems (Post et al., 2013; Wang et al., 2020), and increasing anthropogenic activities (Stephenson et al., 2018). Thus, major uncertainties remain in our understanding of regional and global aerosol sources, their precursors, and their relative importance to depositional efficiency (Willis et al., 2018).

To minimize these uncertainties, aerosol monitoring efforts within the Arctic rely on continuous observations at long-term monitoring stations (Willis et al., 2018), ship and aircraft campaigns (Ancellet et al., 2014; Fisher et al., 2010; Roiger et al., 2015), and source analyses using emission inventories (Giglio et al., 2013; Huang et al., 2015; Randerson et al., 2012; Stohl et al., 2015). These data suggest that 70% of EC emissions within the Arctic are of anthropogenic origin (AMAP, 2015), while globally, only about 40% are anthropogenic. In the High Arctic, coal and diesel remain the primary fuels for transportation and heating, respectively. Another poorly constrained source of EC is gas flaring in the power sector (Stohl et al., 2013). Emission inventories indicate that gas flaring contributes 3% to global EC, but 60–70% to Arctic EC, yet ground observations do not corroborate significant gas flaring emissions (Winiger et al., 2019). In addition, volcanic activity might contribute to the fossil EC burden (Leaitch et al., 2018).

Biomass burning, including wildfires, crop residue burning, and biofuel usage, also contributes to the Arctic's EC burden (Barrett et al., 2015; Mouteva et al., 2015; Warneke et al., 2010; Winiger et al., 2017; Winiger et al., 2019). Biomass burning can inject significant amounts of EC into the free troposphere and stratosphere, which increases the lifetime of EC, particularly when the atmosphere is strongly stratified in winter and spring (Fromm et al., 2010; Qi & Wang, 2019; Stohl et al., 2006). Biomass emissions are greatest between March and October, yet transport to and within the Arctic is limited during the summer by increased wet-scavenging efficiency under warmer and more humid conditions (Browse et al., 2012; Garrett et al., 2011).

During the past three decades, peak concentrations of EC during winter have declined at most Arctic monitoring stations, including Alert (−49%), Barrow (−33%), and Zeppelin (−40%) due to improvements in combustion technology, the use of low emission fuels, and declines in former Soviet Union emissions (AMAP, 2015; Sharma et al., 2006, 2013). Additionally, changes in transport and deposition pathways are expected to reduce Arctic EC by 14% by the end of the 21st century (Jiao & Flanner, 2016) in response to shifts in climate, large-scale weather patterns, increased atmospheric temperatures, and sea-ice regime shifts from thick multiyear ice to thinner first-year ice (Komatsu et al., 2018; Pozzoli et al., 2017; Woods & Caballero, 2016). Nonetheless, major uncertainties remain in respect to quantifying current EC emissions, the rise of ship emissions, and modeling future aerosol-cloud interactions (Willis et al., 2018; Winiger et al., 2019).

Estimating geographical and sector contributions to Arctic EC load usually involves matching observationally based concentrations of EC to modeled outputs derived from emission inventories and meteorology-driven chemical transport models (Qi, Li, Henze, et al., 2017; Qi, Li, Li, & He, 2017). These modeling studies depend on meteorology and a proper description of chemical processing with the

current state of knowledge on EC aging and deposition rates. For the Alert monitoring station, modeling efforts continue to capture the observed seasonal cycle but either overestimate or underestimate EC concentrations year-round (Browse et al., 2012; Qi, Li, Henze, et al., 2017; Qi, Li, Li, & He, 2017) due to uncertainties in emission inventories (AMAP, 2015) and shifting seasonal depositional processes (Browse et al., 2012, 2014).

Another approach for quantifying the sources of carbonaceous aerosol is to measure their stable ($\delta^{13}C$) and radiocarbon ($\Delta^{14}C$) compositions (Heal, 2014; Martinelli et al., 2002). $\delta^{13}C$ signatures reflect mass-dependent fractionation of ^{13}C versus ^{12}C during biogeochemical processes and can be used to differentiate fossil fuels (gaseous vs. liquid/solid). $\Delta^{14}C$ data are corrected for mass-dependent isotopic fractionation, represents a measure of age (or source), and can be used to separate fossil fuel-derived from biomass carbon.

Specifically, ^{14}C is a radioisotope produced in the upper atmosphere with a half-life of 5,730 years. It is oxidized to carbon dioxide (CO_2) and enters the food chain via photosynthesis so that living biomass (and any EC emitted during its combustion) is labeled with the ^{14}C content of the atmospheric CO_2 at growth. When the organism ceases carbon uptake upon death, its $\Delta^{14}C$ declines due to radioactive decay. Consequently, ancient fossil fuels (and their EC emissions) are ^{14}C free ($\Delta^{14}C = -1{,}000‰$). While EC emissions from annual biomass have the same $\Delta^{14}C$ as current atmospheric CO_2, EC from perennial plants reflects the integrated $\Delta^{14}C$ of the atmosphere over their lifetime. This atmospheric $\Delta^{14}C$ has been changing dramatically since 1950, because thermo-nuclear weapon's testing in the mid-20th century doubled the atmosphere's ^{14}C content; biomass formed after 1950 contains additional ^{14}C (bomb or modern ^{14}C, $\Delta^{14}C > 0‰$). The amount of ^{14}C in the atmosphere (and biomass) has been declining over the past 70 years due to mixing of bomb ^{14}C with the ocean and biosphere reservoirs in the global carbon cycle and by dilution with fossil fuel-derived CO_2 (Graven, 2015; Levin et al., 2010).

Measurements of $\Delta^{14}C$ of EC across the Arctic by Winiger et al. (2015, 2016, 2017, 2019) generally support the predictions of EC emission inventories and modeling. Yet low carbon concentrations posed a challenge that in the past have forced these studies to integrate samples for as long as 3 months, particularly during the summer. Here, we present the first time series of $\Delta^{14}C$ of μg-sized EC samples (5–20 μg C) at higher time resolution (13 to 41 days) from aerosol suspended in surface air and scavenged in snow. Specifically, we quantified the composition of carbonaceous aerosols in airborne particulate matter (PM) and snow at Alert, Canada, between March 2014 and June 2015. To elucidate the chemical properties of the aerosol composition, we isolated OC and EC fractions with the ECT9 protocol (Huang et al., 2006, 2020). We also combined $\delta^{13}C$ and $\Delta^{14}C$ mass balance analyses of the EC fraction with backward trajectory modeling (HYSPLIT) to identify aerosol source sectors and regions.

2. Materials and Methods

2.1. Sample Collection

2.1.1. Total Suspended Particles

A custom-built high-volume aerosol sampler was used at the Dr. Neil Trivett Global Atmosphere Watch Observatory at Alert, Canada (83.2°N, 62.5°W, 210 m above sea level) to collect weekly or biweekly samples as part of long-term carbonaceous aerosol observation program. The PM samples used in this study represent total suspended particles and were collected between 5 March 2014 and 3 June 2015. The sampler is installed at a walk-up deck, about 5 m above the ground. Flow rate is approximately 1.4 m^3 min^{-1} at STP conditions. Quartz filters (QFF, Millipore, 8 × 10 in., USA) were sampled continuously with 7-day sampling time from December–April and 14 days from May–November. A total of eight field blanks were measured. After sampling, filters were stored (at room temperature ~20°C) in their sampling cartridges (inside sealed plastic bags) at the Alert station and shipped in aluminum boxes (containing five sampling cartridges each) to Toronto, where they were wrapped in precombusted Al-foil and stored at −30°C until analysis. Air temperatures and pressures were recorded and averaged over the integrated sampling time, and both are used for final flow rate and total air volume calculation.

2.1.2. Snow

Fresh snow was collected from the ground at a fixed location (GPS coordinate: 82.45°N; 62.51°W) about 100 m south of the laboratory throughout a period of 8 months (October 2014 to May 2015). The sampling

strategy was designed to capture fresh snow after snow fall events. Snow was collected into a stainless steel (SS) Dewar (750 ml) using a SS scooper. Each collection was 7–10 days apart. Ideally, three fresh snow samples were collected throughout 1 month evenly distributed in time. If there were no events, however, the collection would capture the same snow as the previous sample. Therefore, it is likely that dry deposition particles and wind-driven drifted snow were also captured. The collected samples in SS dewars were stored in coolers, which were placed outside of the lab until transporting them back to Toronto for EC analysis at the Carbonaceous Aerosol and Isotope Research (CAIR) laboratory within the Climate Research Division (CRD) of Environment and Climate Change Canada (ECCC).

The snow samples were melted individually in a microwave in a glass beaker. The snow water was sonicated and deposited onto quartz filters through filtration. After drying, the filters were analyzed for EC mass concentrations via the ECT9 protocol (see the supporting information for more details).

2.2. Carbonaceous Aerosol Analysis

To determine the concentration and composition of the carbonaceous aerosol, all filters were analyzed with the EnCan-Total-900 (ECT9) protocol on an OC/EC analyzer (Sunset Laboratory Inc.) at CAIR (Chan et al., 2019; Huang et al., 2006). The ECT9 protocol and its application to isotope measurements are discussed in detail in Huang et al. (2020). Briefly, (1) OC is released in pure helium (He) at 550°C for 600 s, (2) pyrolyzed OC (POC) and carbonate carbon (CC) are released in He stream at 870°C for 600 s, and (3) EC is combusted at 900°C in 98% He and 2% oxygen (O_2) for 420 s. CO_2 oxidized from all carbon fractions are then converted to methane (CH_4), and carbon contents were quantified with a flame ionization detector. Each sample is internally calibrated with a known amount of CH_4 at the end of each analysis. The analytical accuracy, precision, and linearity range of the ECT9 method are 0.2, 0.1, and 1–17 μg cm^{-2}, respectively (Huang et al., 2006). The reproducibility of EC/TC ratio is less than 2% (Huang et al., 2020). The concentration of OC was calculated as the sum of OC and POC + CC, while total carbon (TC) was calculated as the sum of the OC, POC + CC, and EC fractions.

In addition, individual EC fractions were analyzed for their $\delta^{13}C$ and $\Delta^{14}C$. To quantify $\delta^{13}C$, the EC fraction was isolated from an additional aliquot of the individual aerosol filters or snow filters with the ECT9 protocol, cryogenically trapped, and measured with the cold-finger mode in an IRMS (MAT 253). The uncertainty of this measurement is about 0.3‰ (Huang et al., 2006, 2020).

For ^{14}C analysis, EC fractions were isolated from additional filter aliquots with the ECT9 protocol, cryogenically trapped, and combined to yield biweekly or monthly integrated samples (Table S1). Similarly, the EC fractions from individual snow events were pooled into monthly integrated samples. Subsequently, the EC fraction (in the form of CO_2) was sent for ^{14}C analysis to the W. M. Keck Carbon Cycle Accelerator Mass Spectrometer (KCCAMS) facility at the University of California, Irvine, USA. Here, the EC-CO_2 samples were purified on a vacuum line and converted to graphite using a sealed-tube zinc reduction protocol for ultrasmall samples (Walker & Xu, 2019) and measured alongside a suite of size-matched (7–34 μg C) and regular-sized (1 mg C) standards (materials with known ^{14}C content). The corresponding processing standards (^{14}C free and modern carbon) were determined, and their ^{14}C contents were corrected for contributions of extraneous carbon (Santos et al., 2007). The total extraneous carbon introduced by EC separation, graphitization, and analysis with accelerator mass spectrometry (AMS) in this study was 1.85 ± 0.62 μg C. EC separation through the ECT9 protocol incorporated on average 0.95 ± 0.47 μg C, while 0.90 ± 0.65 μg C was incorporated through the combustion, graphitization, and AMS analysis (Table S3). Sample sizes ranged from 3.2 to 19.5 μg C and corrected using a mass balance approach, resulting in larger uncertainties for smaller samples (Figures 4 and 5; Table S1). The details of ^{14}C analysis for ultrasmall samples in conjunction with the ECT9 protocol can be found in Huang et al. (2020).

2.3. EC Source Apportionment

EC is a byproduct of incomplete combustion processes. Major EC emission sources include biomass burning and fossil fuels. Therefore, we used two independent approaches to estimate the relative contribution of potential emission sources to the seasonal EC fraction in PM and snow.

First, we used an isotope-mixing model to estimate the relative contributions (f) of fossil ($_{FF}$) versus biomass burning ($_{BB}$) fuel sources to the EC fraction in each sample ($_{SPL}$) of PM and snow (Equation 1). We

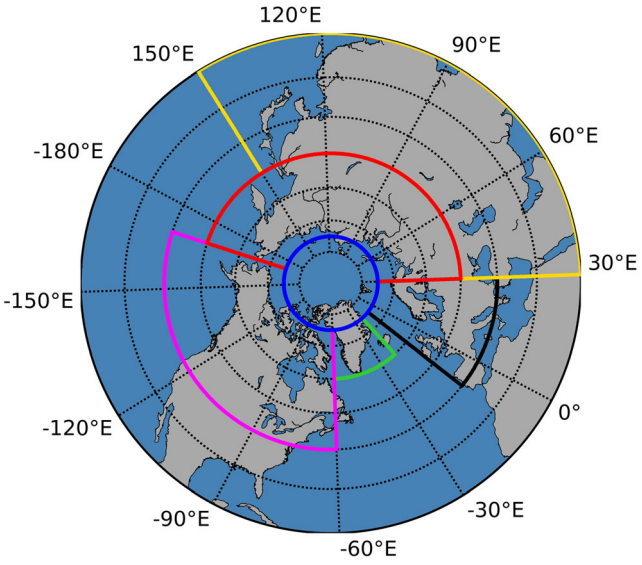

Figure 1. Map of geographical boundaries of six elemental carbon (EC) source regions (Arctic Ocean, Greenland, North America, Russia, Europe, and Asia).

considered EC emission sources with the following $\Delta^{14}C$ values (mean ± SD): combustion of fossil fuels ($\Delta^{14}C = -1{,}000‰$) and (a) annual biomass, which has the same $\Delta^{14}C$ as ambient atmospheric CO_2 ($\Delta^{14}C = 18.2 \pm 3.3‰$ at Pt. Barrow, AK, USA between February 2014 and June 2015 (Xu, Pers. Comm. 2019) or (b) boreal forests in North America, which in previous years incorporated ^{14}C-enriched CO_2 (bomb-C) into their wood ($\Delta^{14}C = 131 \pm 52‰$, Mouteva et al. (2015).

$$f_{FF} = \left(\Delta^{14}C_{SPL} - \Delta^{14}C_{BB}\right) / \left(\Delta^{14}C_{FF} - \Delta^{14}C_{BB}\right) \quad (1)$$

Second, we estimated $\delta^{13}C$ of fossil EC emissions (Equation 2).

$$\delta^{13}C_{FF} = \left(\delta^{13}C_{SPL} - (1 - f_{FF}) \cdot \delta^{13}C_{BB}\right) / f_{FF} \quad (2)$$

Third, we apportioned the fossil fuel-derived EC into gaseous ($_{GAS}$) versus solid or liquid ($_{SOLI}$) fuel sources (Equation 3).

$$f_{GAS} = \left(\delta^{13}C_{FF} - \delta^{13}C_{SOLI}\right) / \left(\delta^{13}C_{GAS} - \delta^{13}C_{SOLI}\right) \quad (3)$$

We assume a $\delta^{13}C$ of $-40 \pm 5‰$ for gaseous sources, based on the combustion of natural gas (Deines, 1980) and gas flaring (−36‰ to −40‰; Winiger et al., 2016). For nongaseous sources, we estimate a $\delta^{13}C$ of $-27 \pm 4‰$. These include the combustion of coal with a $\delta^{13}C$ of $-23.4 \pm 1.3‰$ and of liquid fuels (gasoline, diesel, and kerosene) with estimated ranges from −23.8‰ to −31.3‰ (Andersson et al., 2015; Mašalaitė et al., 2012; Pugliese et al., 2017).

2.4. HYSPLIT Back Trajectory Modeling

We estimated the origin of the air masses at Alert using the HYSPLIT backward trajectory model (Stein et al., 2015) using daily files archived meteorological forecasts containing 3-hourly data from the Global Data Assimilation System (GDAS) at a 0.5°-resolution grid (https://www.ready.noaa.gov/archives.php). While the estimate lifetime of EC in the Arctic ranges from 7–23 days (Qi, Li, Li, & He, 2017), we initialized simulations every 12 hr and calculated air mass geographical position and height back to 240 hr before initialization. Backward trajectories were then pooled to match isotope sampling dates (Table S1) and segregated by meteorological season. Air masses were further distinguished into six geographical source regions (Arctic Ocean, Greenland, North America, Russia, Europe, and Asia; Figure 1; Table S2) by counting the frequency of trajectory intersections over the geographical grids of 1° × 1° resolution. These frequencies were then normalized by the total number of trajectories and mapped (Figure 2).

Arctic geographical and height sectors were analyzed by separating HYSPLIT output endpoints by major Arctic sector and calculating the percentage of each sector in each sample. The planetary boundary layer height was obtained for each endpoint location and time from the GDAS 0.5° meteorology data. The endpoints were binned by height layer in each sector. The height layers include (1) within boundary layer, (2) below 1 km, and (3) 1 to <2 km.

3. Results and Discussion

3.1. Air Mass Origin

Our 10-day backward trajectories indicate that EC in PM and snow was transported to Alert primarily from within the Arctic (>60°N) (Figure 2). This is consistent with previous studies (Schulz et al., 2019; Sobhani et al., 2018; Thomas et al., 2019) showing that, due to the highly stratified nature of the Arctic atmosphere, most air masses at the surface level are contained within the boundary layer and are primarily influenced laterally by air masses with cyclonic flow around the pole.

Seasonally integrated trajectories (Figure 2) also show the contraction of the polar dome during the summer and its expansion during the winter, when there is a greater incidence of air masses within the Arctic and

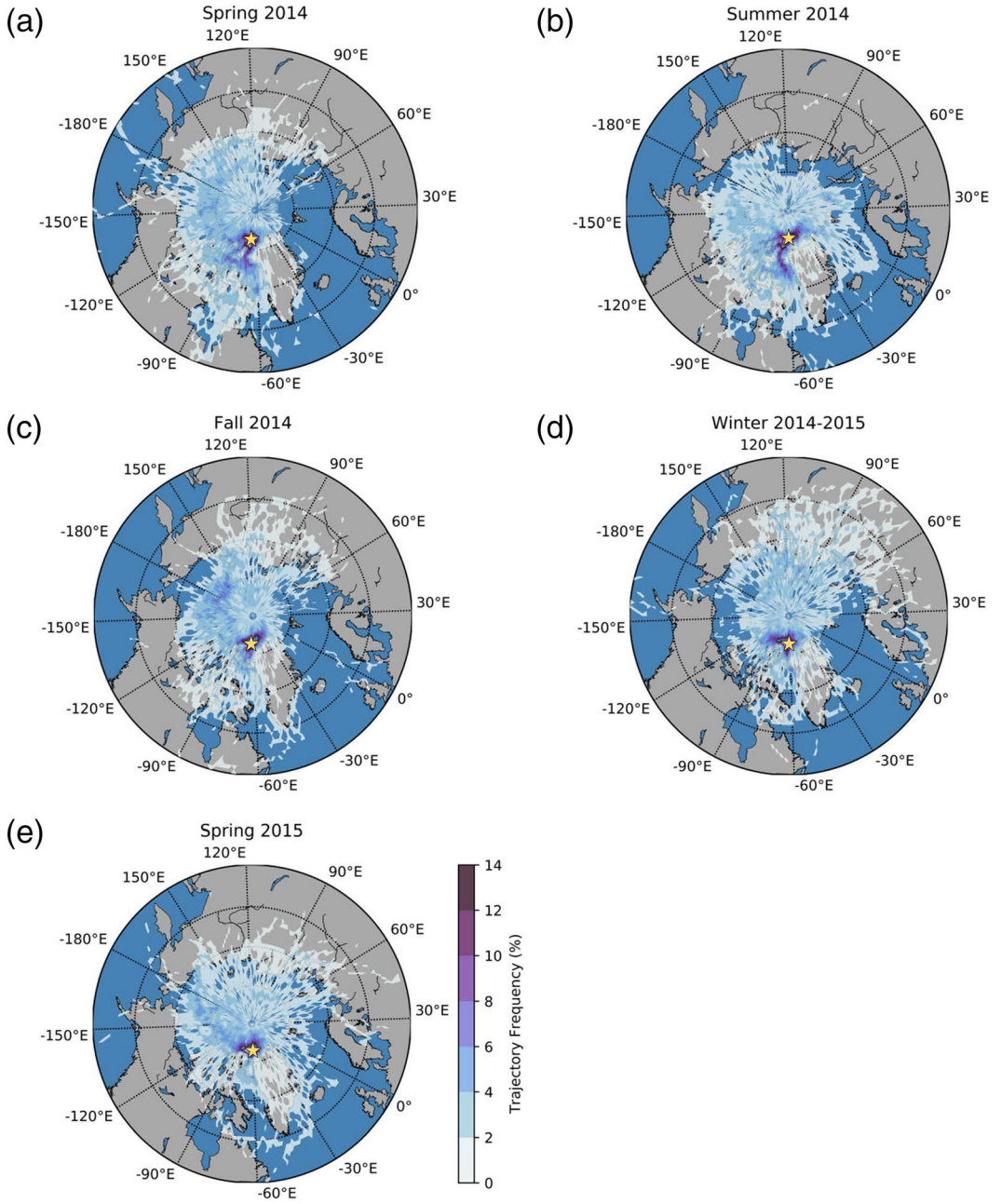

Figure 2. Seasonal (a–e) HYSPLIT backward trajectory frequency maps (see section 2.4) normalized by total trajectory endpoints. Frequency normalized for each 1° × 1° grid cell and initialized every 12 hr for 240 hr (10 days) during sampling at Alert, Canada (82.499°N, 62.342°W).

northern midlatitudes (50–70°N). The polar dome expands asymmetrically into the Russian and Eurasian sectors and to a lesser extent into the European sector. As a result, the air masses simulated for 10 days may not encapsulate all midlatitude sources where the polar dome extends further south, such as in the Asian section. Winter and spring air masses arriving at Alert appear to originate predominantly from the Russian sector as far as 10 days back, but more southern sources cannot be ruled out (Xu et al., 2017). Summer air masses arrive from the North American sector, and predominant wind patterns isolate Alert from direct European emissions year-round.

Table 1
Seasonal Averages of Measured TC, OC, and EC Concentrations and Isotopes (mean ± SD)

	n	OC	EC	TC	OC/EC	EC/TC	*n*	$\delta^{13}C$	$\Delta^{14}C$
		ng C m^{-3} air			%			‰	
					PM				
Spring	23	259.2 (163.0)	40.8 (27.8)	300.1 (180.8)	7.1 (2.9)	15.1 (8.8)	7	−27.2 (0.4)	−581 (78.7)
Summer	9	172.1 (100.2)	14.4 (13.3)	169.7 (103.3)	13.0 (9.2)	8.9 (6.5)	3	−26.2 (0.8)	−361.8 (162.7)
Fall	6	156.0 (78.7)	29.8 (30.5)	185.8 (102.0)	6.8 (3.4)	15.0 (6.5)	5	−27.9 (0.5)	−593.5 (63.6)
Winter	10	324.0 (110.4)	82.3 (29.8)	406.2 (135.6)	4.1 (1.0)	20.2 (3.6)	5	−27.2 (0.3)	−591.4 (100.1)
					Snow				
Spring	n.m.	n.m.	n.m.	n.m.	n.m.	n.m.	3	−27.4 (0.8)	−323.2 (115.5)
Summer	n.m.	n.m.	n.m.	n.m.	n.m.	n.m.	n.m.	n.m.	n.m.
Fall	n.m.	n.m.	n.m.	n.m.	n.m.	n.m.	1	−28.3	−106.2
Winter	n.m.	n.m.	n.m.	n.m.	n.m.	n.m.	3	−27.1 (1.1)	−341.7 (149.8)

Note. Seasons are defined meteorologically, with spring (March–May), summer (June–August), fall (September–November), and winter (December–February); n.m. = not measured (no samples available). OC concentrations are reported as OC_{total}, the sum of OC and pyrolized organic carbon (POC; Huang et al., 2020).

Monthly composite means of sea level pressure (Figure S1) further indicate that asymmetric synoptic-scale meteorology isolates Alert from European emissions and enhances air mass incidences from Russia during winter, spring, and fall while North America air masses were enhanced in summer. Our observations are consistent with previous synoptic-scale patterns described for the Arctic (Cassano et al., 2006; Serreze et al., 1993; Serreze & Barry, 1988) and at Alert (Leaitch et al., 2018; Sharma et al., 2006).

3.2. Concentrations of TC, EC, and OC in PM

Concentrations of TC, EC, and OC in PM ranged from 35.3 to 697.9, 1.8 to 135.3, and 22.6 to 590.6 ng C m^{-3} air, respectively (Table S4). As such, EC/TC ratios ranged from 0.02 to 0.41, and OC/EC ratios ranged from 1.4 to 50.5 (Table S4). TC was mostly composed of OC (58.8–98.1% TC), with EC accounting for 1.9–41.2% TC. These data are consistent with previous measurements at Alert (Croft et al., 2016; Evangeliou et al., 2016; Qi, Li, Li, & He, 2017; Sharma et al., 2017; Sobhani et al., 2018; Winiger et al., 2019).

EC and OC concentrations varied seasonally, with maxima in late winter and early spring (February–April) and minima in early summer (Table 1; Figures 3 and 4a). EC concentrations for winter 2014/2015 were 1.8–2.2 times greater than in spring, 4.8 times greater than in summer, and 2.8 times greater than in fall (Figure 3) ($p < 0.05$). This seasonal cycle is consistent with previous observations (Gong et al., 2010; Sharma et al., 2006). Greater EC concentrations in winter have been shown to arise from increases in

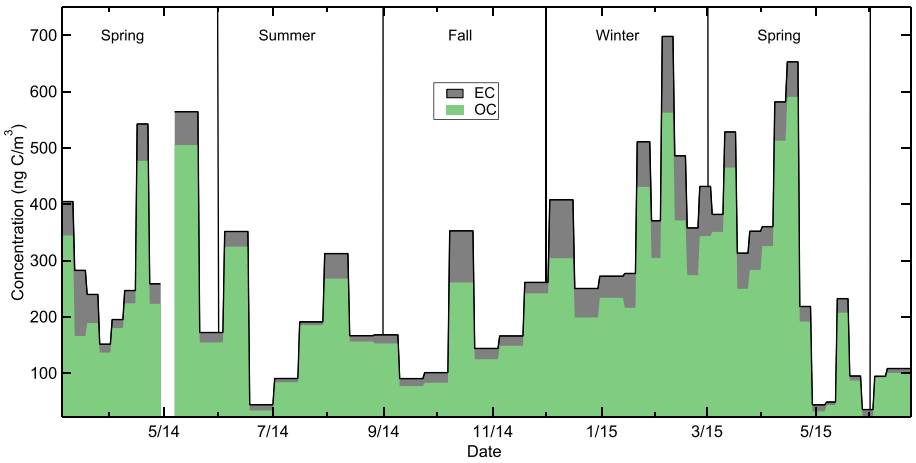

Figure 3. Weekly integrated mass of total organic carbon in PM (bars) at Alert, Canada), composed of the sum of organic carbon (OC), pyrolyzed and carbonate carbon (POC + CC), and elemental carbon (EC). The sum of the OC, POC + CC, and EC fractions equals the mass of total carbon (TC) in each sample.

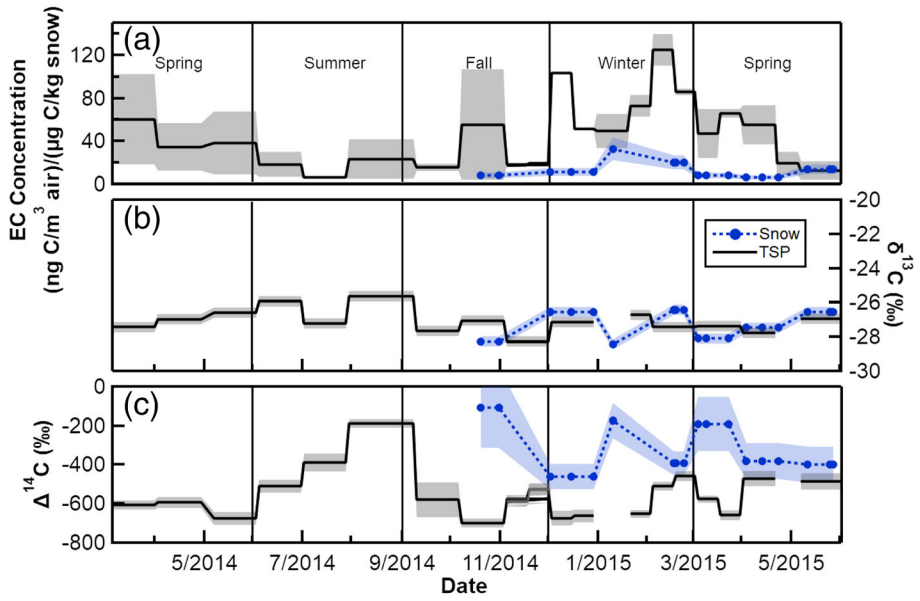

Figure 4. Concentration, stable isotope composition ($\delta^{13}C$), and radiocarbon content ($\Delta^{14}C$) of elemental carbon (EC) from PM (black solid lines) or snow (blue dotted lines) collected at Alert, Canada, and isolated by the ECT9 method. PM concentrations were measured on weekly integrated samples (Figure 3) but pooled for isotope analysis (1–4 weeks/sample). (a) Average EC concentrations and standard deviations (shading) of the pooled samples. Measured (b) $\delta^{13}C$ and (c) $\Delta^{14}C$ of EC with $\pm 1\sigma$ analytical error (shading). Blue dots indicate snow sampling dates.

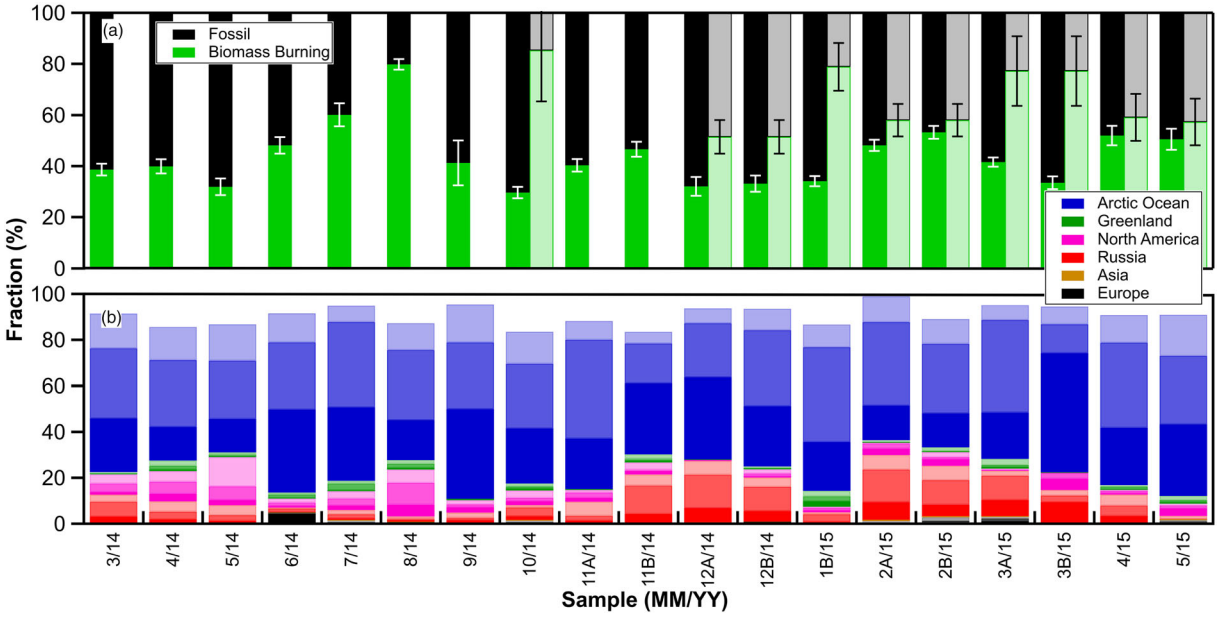

Figure 5. (a) Time series of calculated fuel type of EC in PM (nonopaque) and snow (opaque) based on ^{14}C measurements; (b) sector and height contributions based off 10-day HYSPLIT back trajectory results. Solid colors in (b) represent percentage of back trajectories within the meteorologically defined planetary boundary level height. Less-opaque colors indicate back trajectories above boundary level height but are lower than 1 km. The least-opaque colors show back trajectories between 1 and 2 km in height. From November 2014 to March 2015, two isotopic measurements were made in the same month. A and B in sample dates distinguish samples taken in the first half from the second half of the month.

emissions within the Arctic as a result of greater anthropogenic demand for heating (Huang et al., 2015; Stohl et al., 2013; Yttri et al., 2014), the southward expansion of the Arctic front (Bozem et al., 2019), and an increase in EC atmospheric lifetime due to inefficient scavenging during cold and stagnant atmospheric conditions (Mouteva et al., 2017; Thomas et al., 2019).

OC concentrations followed similar seasonal trends, but differences were not statistically significant (ANOVA, Tukey HSD Post-Hoc Test) because the maxima and minima occurred over more than one season. For example, post-Arctic haze OC minima occurred midsummer of 2014, but late spring the following year (Figure 3). These sudden declines in total carbonaceous aerosol concentration have been described as a product of increasing insulation and warmer temperatures that yield increased wet scavenging efficiencies of organics and water-soluble OC and EC resulting from a shift to a warmer mixed-phase and liquid-phase scavenging regime from inefficient ice-phase cloud particle scavenging (Browse et al., 2012).

TC and EC/TC varied greatly throughout the sampling period without statistically significant seasonal trends. Samples measured in summer had greater OC/EC ratios because EC concentrations were lowest in summer on average. The summer average OC/EC ratio was 3.1 times greater than the winter average.

We also observed three periods of elevated EC concentrations throughout the observation period (Figures 3 and S3), which we defined as EC concentrations $\geq 2\sigma$ from the seasonal average (Table 1). The first occurred in spring 2014 (12–19 March 2014, 2.2σ), the second in summer 2014 (30 July to 13 August 2014, 2.0σ), and the third in fall 2014 (8–22 October 2014, 2.0σ).

We observed the highest overall EC concentrations in winter 2015 (135.8 ng C m^{-3} and 114.7 ng m^{-3} during 4–11 and 11–18 February 2015, respectively), but they were only 1.8 and 1.1σ greater than the seasonal average. Both periods coincided with the development of persistent large high-pressure systems, the center of which oscillated between the east Russian and North American regions throughout winter and spring, that enveloped the entirety of east Russia and west North America (Figure S1). Additionally, an opposing large low-pressure system centered over the Barents and Greenland seas created a sharp pressure gradient at the center of the Arctic Ocean and fueled trans-Arctic Ocean winds from east Russia to Alert (Figure S1n). Similar sea level pressure patterns were observed during periods with elevated EC concentrations throughout winter and spring 2014/2015 (Figure S1k–S1q). These conditions describe typical Arctic winter and springtime temperature inversion events, which are characterized by minimized vertical mixing and stable atmospheric conditions near the surface which drives EC accumulation in the polar dome at the surface (Qi, Li, Henze, et al., 2017; Shen et al., 2017; Thomas et al., 2019).

Surface EC concentrations at Alert closely followed expected seasonal variations of air mass origin as described by backward trajectory modeling and predominant synoptic-scale meteorology in the polar dome. In addition, our sampling approach captured air masses with elevated EC concentrations, each affecting Alert for up to 2 weeks, which suggests either anomalous flow not captured in the means or sudden increases in emissions from respective air mass sources.

3.3. Isotopes of EC in PM

$\Delta^{14}C$ of EC in PM ranged from −698.3‰ to −187.7‰, indicating that overall fossil fuel combustion was the largest contributor to the EC burden at Alert in winter (Table S1; Figure 4c). EC was more enriched in ^{14}C during the summer (Table 1).

The relative contribution from fossil fuel combustion to EC ranged from 20–70% and was significantly lower in summer (Figure 5a) (summer: 20–52% fossil; fall-spring: 47–70% fossil). This indicates a greater contribution from biomass burning, which is expected during the boreal region wildfire season (May–September) (Warneke et al., 2010). Throughout spring and winter, the Russian sector was a significant contributor to the EC load at Alert (Figure 5b), because large persistent anticyclonic systems (Figure S1) envelop the western Arctic in contrast with large cyclonic systems over the eastern Arctic. These conditions present frigid and dry conditions (Figure S2) that limit wet scavenging and drive trans-Arctic ocean winds from Siberia to Alert.

Our EC source apportionment calculations assume that modern carbon emission originated primarily from the burning of annual biomass. As a sensitivity test for the calculated fuel-type contributions expressed in Figure 5a, we calculated the fuel fractions with boreal forest fire endmember ($\Delta^{14}C = 131 \pm 52$‰) (Mouteva et al., 2015) as the biogenic modern carbon source. We found that using a boreal forest fire

endmember only reduced our estimate of biogenic contributions by 4 ± 1% (avg ± sd) on average and by up to 8% for samples with more enriched ^{14}C signatures (collected in summer). These differences in biogenic contributions were within the propagated uncertainty (Figure 5a) and did not significantly affect the calculated fuel type.

Regarding the three elevated EC periods described in section 3.2, $\Delta^{14}C$ EC during the spring and fall events were consistent with that of EC during the respective season (Figure 4c). In spring (March 2014), influent sectors, mean winds, and sea level pressures indicate a steep pressure gradient between a high pressure centered over the Chukchi and Beaufort seas and a low pressure settled over the Kara and Barents seas that drove winds to Alert from the Russian sector via the Arctic Ocean (Figure S1a). A similar pattern was observed in fall (October 2014), but mean sea level pressure gradients were not as steep, the high pressure was contained to the Arctic Ocean, and the low pressure was shifted toward the Norwegian Sea (Figure S1h). Therefore, Alert was affected less by the Russian Sector. Backward trajectories also indicate less Russian influence and less overall influence from air masses within 2 km (Figure 5). This could be due to subsidence occurring at the high-pressure system therefore descending pollution, if any, from aloft (Willis et al., 2019).

In contrast, $\Delta^{14}C$ during the elevated EC event in summer (August 2014) was enriched relative to the seasonal average (Figure 4c). During the event, a regional and weak low-pressure system developed over the Canadian Archipelago (Figure S1f) which drove southwesterly winds from the North American boreal zones, resulting in elevated EC concentrations with relatively high ^{14}C contents (Figures 4a and 4c). This was further evident by increased incidences of back trajectories from North America in in July and August (Figure 5b).

Biomass burning contributed 43.8 ± 11.9% (avg ± 1σ) to EC ($n = 17$) on average for the entire study period. This estimate is within the range of values reported for Alert by Winiger et al. (2019), who estimated an average fraction biomass for EC of 39.6 ± 4.0% (12 February 2014 to 18 March 2015, $n = 9$). Winiger et al. (2019) utilizes more enriched ^{14}C values (+225 ± 60‰) for their biomass burning endmember to represent the ^{14}C content of northern tree species that are 3–4 decades old and contain a significant fraction of bomb ^{14}C, while our approach assumes that fire consumes only the most recently formed wood on the outer stems and carbon from the forest floor that is more depleted in bomb ^{14}C (Mouteva et al., 2015). However, since most EC emissions originate from fossil fuels, the apportionment is not very sensitive to the choice of biomass $\Delta^{14}C$.

The $\delta^{13}C$ of EC in PM ranged from −25.6‰ to −28.3‰ (Table S1; Figure 4b). We observed the most depleted values during the fall, but seasonal differences were not significant (single-factor ANOVA, Tukey HSD test, $p > 0.05$). Our data were similar to $\delta^{13}C$ of EC in PM previously reported for Alert (−27.9 ± 0.8‰, 5 March 2014 to 18 March 2015) (Winiger et al., 2019). Additionally, these data fall within the range of reported $\delta^{13}C$ values of particles produced by fossil fuel combustion (−24‰ to −28‰) (Andersson et al., 2015; Mašalaitė et al., 2012; Pugliese et al., 2017; Widory, 2006) and overlaps with $\delta^{13}C$ values found in biomass burning aerosols (−21‰ to −29‰) (Agnihotri et al., 2011; Garbaras et al., 2015; Mouteva et al., 2015; Sang et al., 2012).

The calculated $\delta^{13}C$ of fossil fuel-derived EC in PM showed little variation throughout the observation period and was not significantly different from the measured $\delta^{13}C$ of bulk EC (Figure 4b; Table S1). Our stable isotope mass balance analysis indicated that the dominant source of fossil EC year-round was the combustion of liquid and solid fuels (82% to 100% of fossil EC). Consequently, gas flaring contributed 0% to 18% to fossil EC, with uncertainties in the isotopic composition of sources and error propagation (Table S1). Our estimates are lower than those by Stohl et al. (2013), who suggested that flaring accounts for as much as 33% to the annual mean EC surface concentrations at Alert in January. However, our gas flaring estimate is greater than that reported by Winiger et al. (2017, 2019), who estimated only 6% contribution from gas flaring in East Siberia to the Tiksi Hydrometeorological Research Observatory and no discernable contribution to Alert.

3.4. Isotopes of EC in Snow

EC in snow was consistently enriched in ^{14}C relative to that of EC in PM (Figure 4c) (ANOVA single factor, $p < 0.01$). This suggests that EC in snow was dominated by biomass burning (53–88%), with $\Delta^{14}C$ ranging from −106.2‰ to −460.2‰ with no significant differences between seasons.

Excluding samples with a fossil EC mass of less than 0.2 μg C, the calculated $\delta^{13}C$ data of fossil fuel-derived EC in snow was relatively constant and not significantly different from the measured $\delta^{13}C$ of bulk EC

(Figure 4b; Table S1). $\delta^{13}C$ values are typical for combustion either from solid or liquid fossil fuels, which accounted for 91% to 100% of fossil EC (avg. ± SD).

The relative enrichment of biomass burning-derived EC in snow compared to that in surface PM likely results from differences in the source region between the EC present aloft and near the surface. EC aloft may be derived from air masses that were directly affected by biomass burning at lower latitudes and uplifted during their northward transport (Bozem et al., 2019; Stohl et al., 2006, 2007), while EC near the surface is dominated by fossil EC emissions within the polar dome.

Biomass burning-derived EC aloft is also likely to be more efficiently scavenged by precipitation. EC scavenging may occur in ice clouds or in liquid and mixed-phase clouds that persist throughout the year in the Alert region as demonstrated at Eureka, Nunavut (Coopman et al., 2018; Cox et al., 2014; de Boer et al., 2011; Morrison et al., 2012).

Current field measurements and laboratory experiments (Bond et al., 2013; Kanji et al., 2017) have shown that EC aerosols are only moderately effective ice nuclei (IN) and easily outcompeted by other IN (Cziczo et al., 2013; Irish et al., 2019; Lupi et al., 2014). However, the lower temperature origin of biomass burning EC and atmospheric aging during transport promote the development of amorphous organic and/or sulfate coatings that increase the solubility of EC in the liquid phase, and its effectiveness as cloud condensation nuclei (CCN) (Henning et al., 2012; Pósfai et al., 2004; Sharma et al., 2013; Zhang et al., 2008).

In mixed-phase clouds, EC may thus act as CCN or become incorporated into existing liquid or supercooled droplets through direct collisions (Ding et al., 2019). Further, the collision of droplets with snow grains ("rimming") can incorporate EC into snow within and below the cloud (Magono et al., 1979). Similarly, aged fossil particles with coatings accumulated through atmospheric processing (China et al., 2015; Weingartner et al., 1997; Zhang et al., 2008; Zuberi, 2005) may be incorporated into snow alongside the biomass burning-derived EC aloft.

We observed the largest differences between the ^{14}C of EC in PM and snow in October 2014 and January and March 2015 (Figure 5a), while the ^{14}C of EC in snow in February, April, and May of 2015 were within the uncertainty range of ^{14}C of EC in PM. Assuming that the majority of snow samples represents fresh snow, the temporal variation in the difference between ^{14}C of EC in PM and snow may suggest a greater layer of complexity that is a function of the atmospheric column conditions. Besides difference in IN capacity, it is also possible that the discrepancy in biomass burning EC particles in snow and PM are due to variability in the extent of contact freezing. Extensive contact freezing of ambient EC-containing particles into existing ice crystals might incorporate more local PM particles, which would yield similar fraction fossil values to ambient PM as was observed in February, April, and May 2015 (Figure 5a).

Our results imply that biomass burning EC is preferentially incorporated into snow. However, this effect is inconsistent across the study period and is likely a function of the specific meteorological and microphysical properties of the precipitating cloud. This study highlights the need for in-depth studies of EC in-cloud behavior as CCN and/or subsequent IN in mixed-phase clouds and measurements of additional biomass burning tracers (i.e., potassium) in snow to assess EC sources. This is particularly important in the Arctic as EC in snow significantly affects the optical properties in snow and yields current uncertainties of the secondary effects of EC in snow (AMAP, 2015; Bond et al., 2013; Schwarz et al., 2013).

4. Conclusions

In this study, we quantified the concentration and sources of EC in PM and snow at Alert, Canada, from March 2014 to May 2015. We found that EC concentrations in PM followed typical seasonal patterns. Throughout the winter, EC accumulated within the polar dome and was predominantly derived from liquid or solid fossil fuels. As far as 10 days back, EC was transported to Alert from the Russian Arctic, but more southern sources may also be important. During late spring and summer, EC concentrations were lower, with greater contributions from biomass burning in North America.

A comparison of EC in PM and snow showed that biomass burning EC was preferentially incorporated into snow. Since EC surface observing networks monitor EC in PM, but not snow, our findings also suggest that EC contributions from biomass burning might be underestimated in models and EC mitigation efforts due to

complexity in transport patterns. Given the effect of EC trapped in snow on Arctic climate, future studies are needed to resolve the relative significant of EC scavenging by dry versus wet deposition and the role of EC in cloud and ice nucleation.

Conflict of Interest

The authors declare no conflicts of interests.

Data Availability Statement

All data measured for this study are available in the figures and tables (including the supporting information) of this manuscript and have been archived at the U.S. National Science Foundation Arctic Data Center (https://doi.org/10.18739/A2QV3C48N).

Acknowledgments
We thank the KCCAMS staff for supporting isotope analyses; A. Platt, M. Fraser, and D. Veber at ECCC for supporting aerosols and snow sampling and maintenance at Alert GAW station; and P. Winiger from Stockholm University for filter preparation.

References

Agnihotri, R., Mandal, T. K., Karapurkar, S. G., Naja, M., Gadi, R., Ahammmed, Y. N., et al. (2011). Stable carbon and nitrogen isotopic composition of bulk aerosols over India and northern Indian Ocean. *Atmospheric Environment*, *45*(17), 2828–2835. https://doi.org/10.1016/j.atmosenv.2011.03.003

AMAP (2015). *AMAP assessment 2015: Black carbon and ozone as Arctic climate forcers*. Oslo, Norway: Arctic Monitoring and Assessment Programme (AMAP). Retrieved from https://www.amap.no/documents/doc/amap-assessment-2015-black-carbon-and-ozone-as-arctic-climate-forcers/1299

Ancellet, G., Pelon, J., Blanchard, Y., Quennehen, B., Bazureau, A., Law, K. S., & Schwarzenboeck, A. (2014). Transport of aerosol to the Arctic: Analysis of CALIOP and French aircraft data during the spring 2008 POLARCAT campaign. *Atmospheric Chemistry and Physics*, *14*(16), 8235–8254. https://doi.org/10.5194/acp-14-8235-2014

Andersson, A., Deng, J., Du, K., Zheng, M., Yan, C., Sköld, M., & Gustafsson, Ö. (2015). Regionally-varying combustion sources of the January 2013 severe haze events over eastern China. *Environmental Science & Technology*, *49*(4), 2038–2043. https://doi.org/10.1021/es503855e

Andreae, M. O., & Gelencsér, A. (2006). Black carbon or brown carbon? The nature of light-absorbing carbonaceous aerosols. *Atmospheric Chemistry and Physics*, *6*(10), 3131–3148. https://doi.org/10.5194/acp-6-3131-2006

Barrett, T. E., Robinson, E. M., Usenko, S., & Sheesley, R. J. (2015). Source contributions to wintertime elemental and organic carbon in the Western Arctic based on radiocarbon and tracer apportionment. *Environmental Science and Technology*, *49*(19), 11,631–11,639. https://doi.org/10.1021/acs.est.5b03081

Bond, T. C., Doherty, S. J., Fahey, D. W., Forster, P. M., Berntsen, T., Deangelo, B. J., et al. (2013). Bounding the role of black carbon in the climate system: A scientific assessment. *Journal of Geophysical Research: Atmospheres*, *118*, 5380–5552. https://doi.org/10.1002/jgrd.50171

Box, J. E., Colgan, W. T., Christensen, T. R., Schmidt, N. M., Lund, M., Parmentier, F.-J. W., et al. (2019). Key indicators of Arctic climate change: 1971–2017. *Environmental Research Letters*, *14*(4), 045010. https://doi.org/10.1088/1748-9326/aafc1b

Bozem, H., Hoor, P., Kunkel, D., Köllner, F., Schneider, J., Herber, A., et al. (2019). Characterization of transport regimes and the polar dome during Arctic spring and summer using in situ aircraft measurements. *Atmospheric Chemistry and Physics*, *19*(23), 15,049–15,071. https://doi.org/10.5194/acp-19-15049-2019

Browse, J., Carslaw, K. S., Arnold, S. R., Pringle, K., & Boucher, O. (2012). The scavenging processes controlling the seasonal cycle in Arctic sulphate and black carbon aerosol. *Atmospheric Chemistry and Physics*, *12*(15), 6775–6798. https://doi.org/10.5194/acp-12-6775-2012

Browse, J., Carslaw, K. S., Mann, G. W., Birch, C. E., Arnold, S. R., & Leck, C. (2014). The complex response of Arctic aerosol to sea-ice retreat. *Atmospheric Chemistry and Physics*, *14*(14), 7543–7557. https://doi.org/10.5194/acp-14-7543-2014

Cassano, J. J., Uotila, P., & Lynch, A. (2006). Changes in synoptic weather patterns in the polar regions in the twentieth and twenty-first centuries, Part 1: Arctic. *International Journal of Climatology*, *26*(8), 1027–1049. https://doi.org/10.1002/joc.1306

Chan, T. W., Huang, L., Banwait, K., Zhang, W., Ernst, D., Wang, X., et al. (2019). Inter-comparison of elemental and organic carbon mass measurements from three North American national long-term monitoring networks at a co-located site. *Atmospheric Measurement Techniques*, *12*(8), 4543–4560. https://doi.org/10.5194/amt-12-4543-2019

China, S., Scarnato, B., Owen, R. C., Zhang, B., Ampadu, M. T., Kumar, S., et al. (2015). Morphology and mixing state of aged soot particles at a remote marine free troposphere site: Implications for optical properties. *Geophysical Research Letters*, *42*, 1243–1250. https://doi.org/10.1002/2014GL062404

Comiso, J. C. (2012). Large decadal decline of the Arctic multiyear ice cover. *Journal of Climate*, *25*(4), 1176–1193. https://doi.org/10.1175/JCLI-D-11-00113.1

Coopman, Q., Garrett, T. J., Finch, D. P., & Riedi, J. (2018). High sensitivity of Arctic liquid clouds to long-range anthropogenic aerosol transport. *Geophysical Research Letters*, *45*, 372–381. https://doi.org/10.1002/2017GL075795

Cox, C. J., Turner, D. D., Rowe, P. M., Shupe, M. D., & Walden, V. P. (2014). Cloud microphysical properties retrieved from downwelling infrared radiance measurements made at Eureka, Nunavut, Canada (2006–09). *Journal of Applied Meteorology and Climatology*, *53*(3), 772–791. https://doi.org/10.1175/JAMC-D-13-0113.1

Croft, B., Martin, R. V., Richard Leaitch, W., Tunved, P., Breider, T. J., D'Andrea, S. D., & Pierce, J. R. (2016). Processes controlling the annual cycle of Arctic aerosol number and size distributions. *Atmospheric Chemistry and Physics*, *16*(6), 3665–3682. https://doi.org/10.5194/acp-16-3665-2016

Cziczo, D. J., Froyd, K. D., Hoose, C., Jensen, E. J., Diao, M., Zondlo, M. A., et al. (2013). Clarifying the dominant sources and mechanisms of cirrus cloud formation. *Science*, *340*(6138), 1320–1324. https://doi.org/10.1126/science.1234145

de Boer, G., Morrison, H., Shupe, M. D., & Hildner, R. (2011). Evidence of liquid dependent ice nucleation in high-latitude stratiform clouds from surface remote sensors. *Geophysical Research Letters*, *38*, L01803. https://doi.org/10.1029/2010GL046016

Deines, P. (1980). The isotopic composition of reduced organic carbon. In P. Fritz & J. C. Fontes (Eds.), *Handbook of environmental isotope geochemistry* (Chap. 9, Vol. 1, pp. 329–406). Amsterdam: Elsevier.

Ding, S., Zhao, D., He, C., Huang, M., He, H., Tian, P., et al. (2019). Observed interactions between black carbon and hydrometeor during wet scavenging in mixed-phase clouds. *Geophysical Research Letters*, *46*, 8453–8463. https://doi.org/10.1029/2019GL083171

Dutkiewicz, V. A., DeJulio, A. M., Ahmed, T., Laing, J., Hopke, P. K., Skeie, R. B., et al. (2014). Forty-seven years of weekly atmospheric black carbon measurements in the Finnish Arctic: Decrease in black carbon with declining emissions. *Journal of Geophysical Research: Atmospheres*, *119*, 7667–7683. https://doi.org/10.1002/2014JD021790

Evangeliou, N., Balkanski, Y., Hao, W. M., Petkov, A., Silverstein, R. P., Corley, R., et al. (2016). Wildfires in northern Eurasia affect the budget of black carbon in the Arctic—A 12-year retrospective synopsis (2002–2013). *Atmospheric Chemistry and Physics*, *16*(12), 7587–7604. https://doi.org/10.5194/acp-16-7587-2016

Fisher, J. A., Jacob, D. J., Purdy, M. T., Kopacz, M., Le Sager, P., Carouge, C., et al. (2010). Source attribution and interannual variability of Arctic pollution in spring constrained by aircraft (ARCTAS, ARCPAC) and satellite (AIRS) observations of carbon monoxide. *Atmospheric Chemistry and Physics*, *10*(3), 977–996. https://doi.org/10.5194/acp-10-977-2010

Fromm, M., Lindsey, D. T., Servranckx, R., Yue, G., Trickl, T., Sica, R., et al. (2010). The untold story of pyrocumulonimbus. *Bulletin of the American Meteorological Society*, *91*(9), 1193–1210. https://doi.org/10.1175/2010BAMS3004.1

Garbaras, A., Masalaite, A., Garbariene, I., Ceburnis, D., Krugly, E., Remeikis, V., et al. (2015). Stable carbon fractionation in size-segregated aerosol particles produced by controlled biomass burning. *Journal of Aerosol Science*, *79*, 86–96. https://doi.org/10.1016/j.jaerosci.2014.10.005

Garrett, T. J., Brattström, S., Sharma, S., Worthy, D. E. J., & Novelli, P. (2011). The role of scavenging in the seasonal transport of black carbon and sulfate to the Arctic. *Geophysical Research Letters*, *38*, LI6805. https://doi.org/10.1029/2011GL048221

Giglio, L., Randerson, J. T., & van der Werf, G. R. (2013). Analysis of daily, monthly, and annual burned area using the fourth-generation global fire emissions database (GFED4). *Journal of Geophysical Research: Biogeosciences*, *118*, 317–328. https://doi.org/10.1002/jgrg.20042

Gong, S. L., Zhao, T. L., Sharma, S., Toom-Sauntry, D., Lavoué, D., Zhang, X. B., et al. (2010). Identification of trends and interannual variability of sulfate and black carbon in the Canadian High Arctic: 1981–2007. *Journal of Geophysical Research*, *115*, D07305. https://doi.org/10.1029/2009JD012943

Graven, H. D. (2015). Impact of fossil fuel emissions on atmospheric radiocarbon and various applications of radiocarbon over this century. *Proceedings of the National Academy of Sciences*, *112*(31), 9542–9545. https://doi.org/10.1073/pnas.1504467112

Hallquist, M., Wenger, J. C., Baltensperger, U., Rudich, Y., Simpson, D., Claeys, M., et al. (2009). The formation, properties and impact of secondary organic aerosol: Current and emerging issues. *Atmospheric Chemistry and Physics*, *9*(14), 5155–5236. https://doi.org/10.5194/acp-9-5155-2009

Hansen, A. D. A., & Rosen, H. (1984). Vertical distributions of particulate carbon, sulfur, and bromine in the Arctic haze and comparison with ground-level measurements at Barrow, Alaska. *Geophysical Research Letters*, *11*(5), 381–384. https://doi.org/10.1029/GL011i005p00381

Heal, M. R. (2014). The application of carbon-14 analyses to the source apportionment of atmospheric carbonaceous particulate matter: A review. *Analytical and Bioanalytical Chemistry*, *406*(1), 81–98. https://doi.org/10.1007/s00216-013-7404-1

Henning, S., Ziese, M., Kiselev, A., Saathoff, H., Möhler, O., Mentel, T. F., et al. (2012). Hygroscopic growth and droplet activation of soot particles: Uncoated, succinic or sulfuric acid coated. *Atmospheric Chemistry and Physics*, *12*(10), 4525–4537. https://doi.org/10.5194/acp-12-4525-2012

Hirdman, D., Burkhart, J. F., Sodemann, H., Eckhardt, S., Jefferson, A., Quinn, P. K., et al. (2010). Long-term trends of black carbon and sulphate aerosol in the Arctic: Changes in atmospheric transport and source region emissions. *Atmospheric Chemistry and Physics*, *10*(19), 9351–9368. https://doi.org/10.5194/acp-10-9351-2010

Huang, K., Fu, J. S., Prikhodko, V. Y., Storey, J. M., Romanov, A., Hodson, E. L., et al. (2015). Russian anthropogenic black carbon: Emission reconstruction and Arctic black carbon simulation. *Journal of Geophysical Research: Atmospheres*, *120*, 11,306–11,333. https://doi.org/10.1002/2015JD023358

Huang, L., Brook, J. R., Zhang, W., Li, S. M., Graham, L., Ernst, D., et al. (2006). Stable isotope measurements of carbon fractions (OC/EC) in airborne particulate: A new dimension for source characterization and apportionment. *Atmospheric Environment*, *40*(15), 2690–2705. https://doi.org/10.1016/j.atmosenv.2005.11.062

Irish, V. E., Hanna, S. J., Willis, M. D., China, S., Thomas, J. L., Wentzell, J. J. B., et al. (2019). Ice nucleating particles in the marine boundary layer in the Canadian Arctic during summer 2014. *Atmospheric Chemistry and Physics*, *19*(2), 1027–1039. https://doi.org/10.5194/acp-19-1027-2019

Jiao, C., & Flanner, M. G. (2016). Changing black carbon transport to the Arctic from present day to the end of 21st century. *Journal of Geophysical Research: Atmospheres*, *121*, 4734–4750. https://doi.org/10.1002/2015JD023964

Kanji, Z. A., Ladino, L. A., Wex, H., Boose, Y., Burkert-Kohn, M., Cziczo, D. J., & Krämer, M. (2017). Overview of ice nucleating particles. *Meteorological Monographs*, *58*, 1.1–1.33. https://doi.org/10.1175/AMSMONOGRAPHS-D-16-0006.1

Komatsu, K. K., Alexeev, V. A., Repina, I. A., & Tachibana, Y. (2018). Poleward upgliding Siberian atmospheric rivers over sea ice heat up Arctic upper air. *Scientific Reports*, *8*(1), 1–15. https://doi.org/10.1038/s41598-018-21159-6

Law, K. S., & Stohl, A. (2007). Arctic air pollution: Origins and impacts. *Science*, *315*(5818), 1537–1540. https://doi.org/10.1126/science.1137695

Leaitch, W. R., Russell, L. M., Liu, J., Kolonjari, F., Toom, D., Huang, L., et al. (2018). Organic functional groups in the submicron aerosol at 82.5°N, 62.5°W from 2012 to 2014. *Atmospheric Chemistry and Physics*, *18*(5), 3269–3287. https://doi.org/10.5194/acp-18-3269-2018

Levin, I., Naegler, T., Kromer, B., Diehl, M., Francey, R., Gomez-Pelaez, A., et al. (2010). Observations and modelling of the global distribution and long-term trend of atmospheric 14CO2. *Tellus Series B: Chemical and Physical Meteorology*, *62*(1), 26–46. https://doi.org/10.1111/j.1600-0889.2009.00446.x

Lupi, L., Hudait, A., & Molinero, V. (2014). Heterogeneous nucleation of ice on carbon surfaces. *Journal of the American Chemical Society*, *136*(8), 3156–3164. https://doi.org/10.1021/ja411507a

Magono, C., Endoh, T., Ueno, F., Kubota, S., & Itasaka, M. (1979). Direct observations of aerosols attached to falling snow crystals. *Tellus*, *31*(2), 102–114. https://doi.org/10.3402/tellusa.v31i2.10415

Martinelli, L. A., Camargo, P. B., Lara, L. B. L. S., Victoria, R. L., & Artaxo, P. (2002). Stable carbon and nitrogen isotopic composition of bulk aerosol particles in a C4 plant landscape of southeast Brazil. *Atmospheric Environment*, *36*(14), 2427–2432. https://doi.org/10.1016/S1352-2310(01)00454-X

Mašalaitė, A., Garbaras, A., & Remeikis, V. (2012). Stable isotopes in environmental investigations. *Lithuanian Journal of Physics*, *52*(3), 261–268. https://doi.org/10.3952/physics.v52i3.2478

Morrison, H., De Boer, G., Feingold, G., Harrington, J., Shupe, M. D., & Sulia, K. (2012). Resilience of persistent Arctic mixed-phase clouds. *Nature Geoscience*, *5*(1), 11–17. https://doi.org/10.1038/ngeo1332

Mouteva, G. O., Czimczik, C. I., Fahrni, S. M., Wiggins, E. B., Rogers, B. M., Veraverbeke, S., et al. (2015). Black carbon aerosol dynamics and isotopic composition in Alaska linked with boreal fire emissions and depth of burn in organic soils. *Global Biogeochemical Cycles*, *29*, 1977–2000. https://doi.org/10.1002/2015GB005247

Mouteva, G. O., Randerson, J. T., Fahrni, S. M., Bush, S. E., Ehleringer, J. R., Xu, X., et al. (2017). Using radiocarbon to constrain black and organic carbon aerosol sources in Salt Lake City. *Journal of Geophysical Research: Atmospheres*, *122*, 9843–9857. https://doi.org/10.1002/2017JD026519

Petzold, A., Ogren, J. A., Fiebig, M., Laj, P., Li, S.-M., Baltensperger, U., et al. (2013). Recommendations for reporting "black carbon" measurements. *Atmospheric Chemistry and Physics*, *13*(16), 8365–8379. https://doi.org/10.5194/acp-13-8365-2013

Pöschl, U. (2005). Atmospheric aerosols: Composition, transformation, climate and health effects. *Angewandte Chemie, International Edition*, *44*(46), 7520–7540. https://doi.org/10.1002/anie.200501122

Pósfai, M., Gelencsér, A., Simonics, R., Arató, K., Li, J., Hobbs, P. V., & Buseck, P. R. (2004). Atmospheric tar balls: Particles from biomass and biofuel burning. *Journal of Geophysical Research*, *109*, D06213. https://doi.org/10.1029/2003JD004169

Post, E., Bhatt, U. S., Bitz, C. M., Brodie, J. F., Fulton, T. L., Hebblewhite, M., et al. (2013). Ecological consequences of sea-ice decline. *Science*, *341*(6145), 519–524. https://doi.org/10.1126/science.1235225

Pozzoli, L., Dobricic, S., Russo, S., & Vignati, E. (2017). Impacts of large-scale atmospheric circulation changes in winter on black carbon transport and deposition to the Arctic. *Atmospheric Chemistry and Physics*, *17*(19), 11,803–11,818. https://doi.org/10.5194/acp-17-11803-2017

Pugliese, S. C., Murphy, J. G., Vogel, F., & Worthy, D. (2017). Characterization of the δ13C signatures of anthropogenic CO_2 emissions in the Greater Toronto Area, Canada. *Applied Geochemistry*, *83*, 171–180. https://doi.org/10.1016/j.apgeochem.2016.11.003

Qi, L., Li, Q., Henze, D. K., Tseng, H. L., & He, C. (2017). Sources of springtime surface black carbon in the Arctic: An adjoint analysis for April 2008. *Atmospheric Chemistry and Physics*, *17*(15), 9697–9716. https://doi.org/10.5194/acp-17-9697-2017

Qi, L., Li, Q., Li, Y., & He, C. (2017). Factors controlling black carbon distribution in the Arctic. *Atmospheric Chemistry and Physics*, *17*(2), 1037–1059. https://doi.org/10.5194/acp-17-1037-2017

Qi, L., & Wang, S. (2019). Sources of black carbon in the atmosphere and in snow in the Arctic. *Science of the Total Environment*, *691*, 442–454. https://doi.org/10.1016/j.scitotenv.2019.07.073

Randerson, J. T., Chen, Y., van der Werf, G. R., Rogers, B. M., & Morton, D. C. (2012). Global burned area and biomass burning emissions from small fires. *Journal of Geophysical Research*, *117*, G04012. https://doi.org/10.1029/2012JG002128

Roiger, A., Thomas, J.-L., Schlager, H., Law, K. S., Kim, J., Schäfler, A., et al. (2015). Quantifying emerging local anthropogenic emissions in the Arctic region: The ACCESS aircraft campaign experiment. *Bulletin of the American Meteorological Society*, *96*(3), 441–460. https://doi.org/10.1175/BAMS-D-13-00169.1

Sang, X. F., Gensch, I., Laumer, W., Kammer, B., Chan, C. Y., Engling, G., et al. (2012). Stable carbon isotope ratio analysis of anhydrosugars in biomass burning aerosol particles from source samples. *Environmental Science & Technology*, *46*(6), 3312–3318. https://doi.org/10.1021/es204094v

Santos, G. M., Southon, J. R., Griffin, S., Beaupre, S. R., & Druffel, E. R. M. (2007). Ultra small-mass AMS 14C sample preparation and analyses at KCCAMS/UCI Facility. *Nuclear Instruments and Methods in Physics Research Section B: Beam Interactions with Materials and Atoms*, *259*(1), 293–302. https://doi.org/10.1016/j.nimb.2007.01.172

Schulz, H., Zanatta, M., Bozem, H., Richard Leaitch, W., Herber, A. B., Burkart, J., et al. (2019). High Arctic aircraft measurements characterising black carbon vertical variability in spring and summer. *Atmospheric Chemistry and Physics*, *19*(4), 2361–2384. https://doi.org/10.5194/acp-19-2361-2019

Schwarz, J. P., Gao, R. S., Perring, A. E., Spackman, J. R., & Fahey, D. W. (2013). Black carbon aerosol size in snow. *Scientific Reports*, *3*(1), 1356. https://doi.org/10.1038/srep01356

Serreze, M. C., & Barry, R. G. (1988). Synoptic activity in the Arctic Basin, 1979–85. *Journal of Climate*, *1*(12), 1276–1295. https://doi.org/10.1175/1520-0442(1988)001<1276:SAITAB>2.0.CO;2

Serreze, M. C., Box, J. E., Barry, R. G., & Walsh, J. E. (1993). Characteristics of Arctic synoptic activity, 1952–1989. *Meteorology and Atmospheric Physics*, *51*(3–4), 147–164. https://doi.org/10.1007/BF01030491

Sharma, S., Ishizawa, M., Chan, D., Lavoué, D., Andrews, E., Eleftheriadis, K., & Maksyutov, S. (2013). 16-year simulation of arctic black carbon: Transport, source contribution, and sensitivity analysis on deposition. *Journal of Geophysical Research: Atmospheres*, *118*, 943–964. https://doi.org/10.1029/2012JD017774

Sharma, S., Andrews, E., Barrie, L. A., Ogren, J. A., & Lavoué, D. (2006). Variations and sources of the equivalent black carbon in the high Arctic revealed by long-term observations at Alert and Barrow: 1989–2003. *Journal of Geophysical Research*, *111*, D14208. https://doi.org/10.1029/2005JD006581

Sharma, S., Richard Leaitch, W., Huang, L., Veber, D., Kolonjari, F., Zhang, W., et al. (2017). An evaluation of three methods for measuring black carbon in Alert, Canada. *Atmospheric Chemistry and Physics*, *17*(24), 15,225–15,243. https://doi.org/10.5194/acp-17-15225-2017

Shaw, G. E., Stamnes, K., & Hu, Y. X. (1993). Arctic haze: Perturbation to the radiation field. *Meteorology and Atmospheric Physics*, *51*(3–4), 227–235. https://doi.org/10.1007/BF01030496

Shen, Z., Ming, Y., Horowitz, L. W., Ramaswamy, V., & Lin, M. (2017). On the seasonality of arctic black carbon. *Journal of Climate*, *30*(12), 4429–4441. https://doi.org/10.1175/JCLI-D-16-0580.1

Sobhani, N., Kulkarni, S., & Carmichael, G. R. (2018). Source sector and region contributions to black carbon and PM2.5 in the Arctic. *Atmospheric Chemistry and Physics*, *18*(24), 18,123–18,148. https://doi.org/10.5194/acp-18-18123-2018

Stein, A. F., Draxler, R. R., Rolph, G. D., Stunder, B. J. B., Cohen, M. D., & Ngan, F. (2015). NOAA's HYSPLIT atmospheric transport and dispersion modeling system. *Bulletin of the American Meteorological Society*, *96*(12), 2059–2077. https://doi.org/10.1175/BAMS-D-14-00110.1

Stephenson, S. R., Wang, W., Zender, C. S., Wang, H., Davis, S. J., & Rasch, P. J. (2018). Climatic responses to future trans-Arctic shipping. *Geophysical Research Letters*, *45*, 9898–9908. https://doi.org/10.1029/2018GL078969

Stohl, A., Aamaas, B., Amann, M., Baker, L. H., Bellouin, N., Berntsen, T. K., et al. (2015). Evaluating the climate and air quality impacts of short-lived pollutants. *Atmospheric Chemistry and Physics*, *15*(18), 10,529–10,566. https://doi.org/10.5194/acp-15-10529-2015

Stohl, A., Andrews, E., Burkhart, J. F., Forster, C., Herber, A., Hoch, S. W., et al. (2006). Pan-Arctic enhancements of light absorbing aerosol concentrations due to North American boreal forest fires during summer 2004. *Journal of Geophysical Research*, *111*, D22214. https://doi.org/10.1029/2006JD007216

Stohl, A., Berg, T., Burkhart, J. F., Fjæraa, A. M., Forster, C., Herber, A., et al. (2007). Arctic smoke—Record high air pollution levels in the European Arctic due to agricultural fires in Eastern Europe in spring 2006. *Atmospheric Chemistry and Physics*, *7*(2), 511–534. https://doi.org/10.5194/acp-7-511-2007

Stohl, A., Klimont, Z., Eckhardt, S., Kupiainen, K., Shevchenko, V. P., Kopeikin, V. M., & Novigatsky, A. N. (2013). Black carbon in the Arctic: The underestimated role of gas flaring and residential combustion emissions. *Atmospheric Chemistry and Physics*, *13*(17), 8833–8855. https://doi.org/10.5194/acp-13-8833-2013

Thomas, M. A., Devasthale, A., Tjernström, M., & Ekman, A. M. L. (2019). The relation between aerosol vertical distribution and temperature inversions in the Arctic in winter and spring. *Geophysical Research Letters*, *46*, 2836–2845. https://doi.org/10.1029/2018GL081624

Walker, B. D., & Xu, X. (2019). An improved method for the sealed-tube zinc graphitization of microgram carbon samples and 14C AMS measurement. *Nuclear Instruments and Methods in Physics Research Section B: Beam Interactions with Materials and Atoms*, *438*, 58–65. https://doi.org/10.1016/j.nimb.2018.08.004

Wang, J. A., Sulla-Menashe, D., Woodcock, C. E., Sonnentag, O., Keeling, R. F., & Friedl, M. A. (2020). Extensive land cover change across Arctic–boreal northwestern North America from disturbance and climate forcing. *Global Change Biology*, *26*(2), 807–822. https://doi.org/10.1111/gcb.14804

Warneke, C., Froyd, K. D., Brioude, J., Bahreini, R., Brock, C. A., Cozic, J., et al. (2010). An important contribution to springtime Arctic aerosol from biomass burning in Russia. *Geophysical Research Letters*, *37*, L01801. https://doi.org/10.1029/2009GL041816

Weingartner, E., Burtscher, H., & Baltensperger, U. (1997). Hygroscopic properties of carbon and diesel soot particles. *Atmospheric Environment*, *31*(15), 2311–2327. https://doi.org/10.1016/S1352-2310(97)00023-X

Widory, D. (2006). Combustibles, fuels and their combustion products: A view through carbon isotopes. *Combustion Theory and Modelling*, *10*(5), 831–841. https://doi.org/10.1080/13647830600720264

Willis, M. D., Bozem, H., Kunkel, D., Lee, A. K. Y., Schulz, H., Burkart, J., et al. (2019). Aircraft-based measurements of high Arctic springtime aerosol show evidence for vertically varying sources, transport and composition. *Atmospheric Chemistry and Physics*, *19*(1), 57–76. https://doi.org/10.5194/acp-19-57-2019

Willis, M. D., Leaitch, W. R., & Abbatt, J. P. D. (2018). Processes controlling the composition and abundance of Arctic aerosol. *Reviews of Geophysics*, *56*(4), 621–671. https://doi.org/10.1029/2018RG000602

Winiger, P., Andersson, A., Eckhardt, S., Stohl, A., & Gustafsson, O. (2016). The sources of atmospheric black carbon at a European gateway to the Arctic. *Nature Communications*, *7*(1), 1–8. https://doi.org/10.1038/ncomms12776

Winiger, P., Andersson, A., Eckhardt, S., Stohl, A., Semiletov, I. P., Dudarev, O. V., et al. (2017). Siberian Arctic black carbon sources constrained by model and observation. *Proceedings of the National Academy of Sciences*, *114*(7), E1054–E1061. https://doi.org/10.1073/pnas.1613401114

Winiger, P., Andersson, A., Yttri, K. E., Tunved, P., & Gustafsson, Ö. (2015). Isotope-based source apportionment of EC aerosol particles during winter high-pollution events at the Zeppelin Observatory, Svalbard. *Environmental Science & Technology*, *49*(19), 11,959–11,966. https://doi.org/10.1021/acs.est.5b02644

Winiger, P., Barrett, T. E., Sheesley, R. J., Huang, L., Sharma, S., Barrie, L. A., et al. (2019). Source apportionment of circum-Arctic atmospheric black carbon from isotopes and modeling. *Science Advances*, *5*(2), eaau8052. https://doi.org/10.1126/sciadv.aau8052

Woods, C., & Caballero, R. (2016). The role of moist intrusions in winter Arctic warming and sea ice decline. *Journal of Climate*, *29*(12), 4473–4485. https://doi.org/10.1175/JCLI-D-15-0773.1

Xu, J. W., Martin, R. V., Morrow, A., Sharma, S., Huang, L., Richard Leaitch, W., et al. (2017). Source attribution of Arctic black carbon constrained by aircraft and surface measurements. *Atmospheric Chemistry and Physics*, *17*(19), 11,971–11,989. https://doi.org/10.5194/acp-17-11971-2017

Yttri, K. E., Lund Myhre, C., Eckhardt, S., Fiebig, M., Dye, C., Hirdman, D., et al. (2014). Quantifying black carbon from biomass burning by means of levoglucosan—A one-year time series at the Arctic observatory Zeppelin. *Atmospheric Chemistry and Physics*, *14*(12), 6427–6442. https://doi.org/10.5194/acp-14-6427-2014

Zhang, R., Khalizov, A. F., Pagels, J., Zhang, D., Xue, H., & McMurry, P. H. (2008). Variability in morphology, hygroscopicity, and optical properties of soot aerosols during atmospheric processing. *Proceedings of the National Academy of Sciences*, *105*(30), 10,291–10,296. https://doi.org/10.1073/pnas.0804860105

Huang, L., Zhang, W., Santos, G. M., Rodríguez, B. T., Holden, S. R., & Czimczik, C. I. (2020). Application of the ECT9 protocol for radiocarbon-based source apportionment of carbonaceous aerosols. *Atmospheric Measurement Techniques Discussions*. https://doi.org/10.5194/amt-2020-201

Zuberi, B. (2005). Hydrophilic properties of aged soot. *Geophysical Research Letters*, *32*, L01807. https://doi.org/10.1029/2004GL021496